Modeling of continuous mixers : the corotating twin-screw extruder

CHAPTER 12

MODELING OF CONTINUOUS MIXERS: THE COROTATING TWIN-SCREW EXTRUDER

H. E. H. Meijer

P. H. M. Elemans

Eindhoven University of Technology
Department of Polymer Technology
The Netherlands

CONTENTS,

INTRODUCTION

In many operations in polymer processing, such as polymer blending, devolatilization, or incorporation of fillers in a polymeric matrix continuous mixers are used, e.g. corotating twin-screw extruders, Buss Co-kneaders and Farrel Continuous Mixers. Theoretical analyses of these machines tend to emphasize the flow in complex geometries rather than generate results which can be directly used [1–5]. In this chapter a simple model is developed for the hot melt closely intermeshing corotating twin-screw extruder, analogous to the analysis of the single screw extruder [6, 7].

Twin-screw extruders may be divided into counter- and corotating types and into closely, partly and nonintermeshing systems [8–10]. Apart from the direction of rotation of the screws they can be subdivided according to their transport mechanism: positive displacement or drag flow. This

division is made by investigating whether the channel is closed in the axial direction (by the flight of the opposite screw) or in fact open [11–13].

Counterrotating extruders are constructed with small clearances. The closely intermeshing types are, therefore, often associated with positive displacement. In practice, this does not prove to be very realistic because apart from the typical tetraheder gap between the sides of the adherent screw flights and the necessary clearance between barrel and screws, the so-called calender gap between screw root and tip of the flight of the opposite screw is often rather large. This gap drags material (with two moving walls) backward into the previous C-shaped chamber. Without this gap, plastification (or gelation) of, for instance, poly(vinyl chloride) (PVC) would be impossible. PVC is often processed with this type of extruder because of the poor transport mechanism in drag extruders (external slip agents). The counterrotating extruder is explained in detail in [14, 15]. The final result is that the pumping characteristic, throughput versus pressure buildup, is rather easily obtained as the number of C-shaped chambers becoming free per unit of time multiplied by the volume of one chamber minus the sum of all leakage flows. Even with small clearances, the backflow, because of leakage, is in the order of half of the positive displacement (depending on the pressure at the die).

Apart from some nonintermeshing types that are sometimes used for devolatilization [16], counterrotating twin-screw extruders can in principle, because of the importance of the calender gap, be treated as a continuous two roll mill process. The analysis of the milling process can be found in any good textbook on polymer processing [17–19].

Analogously, the Farrel Continuous Mixer can be treated as an internal mixer fed by a nonintermeshing counterrotating twin-screw extruder. Although numerous papers have been published on these mixers, especially with respect to rubber compounding, only a few are significant. For example, the work by Noordermeer [20] whose emphasis is on the rubber, following the work originally done by Tokita and White [21, 22] and by Manas et al. [23] who developed the first really interesting model on the dispersive mixing of carbon black in a rubber matrix, an analysis that can easily be extended to other processing equipment or to the mixing of polymer blends [24, 25].

In practice, corotating extruders can also be constructed with broad flights, as is sometimes done in the feed section, to solve problems with difficult-to-transport powders. However, their tetraheder gap is always much larger than the one in counterrotating extruders. Moreover, they are constructed with closely intermeshing screws in order to promote the self-wiping and, as a consequence, the flights leave a completely open 8-shaped chamber. Therefore, the transport mechanism is drag flow. The analysis of the corotating twin-screw extruder can be found in [4], but as in [14, 15] too much effort is paid to a detailed treatment of the complex geometry and the reader becomes easily lost. Rauwendaal [14] pays some attention to the modeling of corotating twin-screw extruders, but the analysis is incomplete and, therefore, of little practical use. Of course, the more important extruder manufacturers have developed their own computer programs to predict the performance of their extruders dependent on screw design and to scale up the results from laboratory measurements to production size [26]. But for reasons that are easily understood, they do not always present their know-how to the competitors in the open literature.

Here, the corotating twin-screw extruder will be dealt with as a single-screw extruder using the theories developed in 1922 and 1928. This is allowed with respect to the transport characteristics of the melt-filled sections because of the completely open channel.

SCREW GEOMETRY

Different screw elements exist. Single-, double- or triple-flighted screws with different pitch, even with negative pitch, mixing and kneading elements. Screw configuration is extremely flexible, a major advantage of this kind of extruder, and can be fitted to the job. At present, mostly double-flighted screw elements are used because of the larger useful volume. Single-flighted screws are less popular because mixing increases with the number of flights.

Although the maximum applicable torque on the screws has been recently doubled in the new series of extruders, the maximum torque is still relatively low in comparison with single-screw extruders and (conical) counterrotating twin-screw extruders. This is inherent to the flexible screw design and self-wiping action. Moreover, a primary task of corotating twin-screw extruders is either

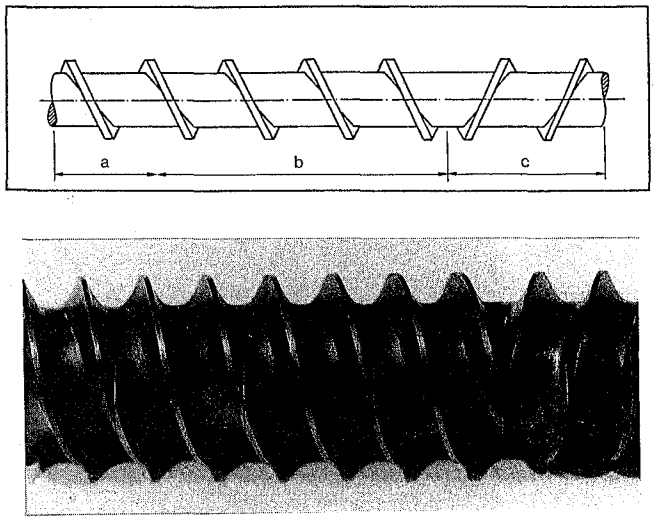

Figure 1. Elementary screw geometry.

to remove volatiles from the melt (water, solvents, monomers) or to add fillers (glass, chalk, talc, mica) via openings in the barrel. As a consequence, all corotating extruders must be underfed, which means that the throughput locally in the open barrel sections is only part of the maximum theoretical throughput. Correct metering of the individual components is often stated to be 80% of the compounding job.

Attention will be focused on the hot melt extruder. In practice, it is used for devolatilization or is present after the melting section in each compounding extruder. Solids conveying, transition and melting sections are difficult to analyze because no distinguished melting mechanism can be recognized as in single-screw extruders [27–30]. Rather a mixture of solids and melt exists as in the dissipative mix melting mechanism [31]. Nevertheless, incorporation of the modeling of the melting section is important because during compounding most of the limited torque is used in this stage of the process. Sometimes even an important part of the dispersive mixing is already achieved here because of the high viscosity (low temperature) of this mixture [32].

The most elementary screw geometry is given in Figure 1 and consists of a sequence of transport elements with positive pitch combined with an element with negative pitch. The principle of the analysis will be explained using this geometry.

In this simplified screwpart, three functional zones are distinguished: part a, partially filled having a degree of fill f ($0 < f < 1$); part b, completely filled, pressure generating; part c, completely filled, pressure consuming. In principle, every screw (some examples are given schematically in Figure 2) is thought to consist of parts "a", "b" and "c". (Local) pressure gradients (following from throughput compared with theoretically maximum throughput) and lengths determine their relative dimensions.

The screw is thought to be stationary and the barrel rotating in the opposite direction as usual. Furthermore, curvatures are neglected by either looking very locally or by unrolling the screw channel. In the first approximation, the screw channel is thought to have a rectangular cross-sectional shape, with average height H and width W. The barrelwall moves with a velocity:

$$V = \pi DN \tag{1}$$

where N is the revolutions per second and D is the diameter over the screw channel under an angle φ, the pitch angle, and drags the liquid into the direction of the die ($|\cos \varphi| \sim 0.95$ neglected here for the time being).

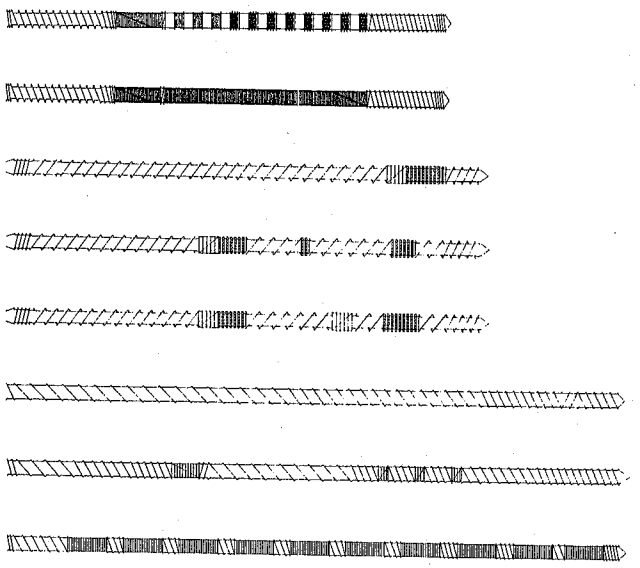

Figure 2. Examples of screw design.

The maximum drag flow capacity in parts "a" is [33]

$$Q_d = \tfrac{1}{2}VHW \tag{2}$$

The real throughput Q is always smaller than Q_d:

$$Q = fQ_d \tag{3}$$

with f the (local) degree of fill, (see Figure 3a). Q is half of the real throughput because only one of the screws is considered here.

Parts "b" are completely filled; therefore $Q_d = \frac{1}{2}VHW$. They are generating pressure, consequently (see Figure 3b)

$$Q = Q_d + Q_p \tag{4}$$

Because the throughput is constant everywhere, the pressure flow equals

$$Q_p = -(1 - f)Q_d \tag{5}$$

Parts "c" are completely filled and consume pressure because the drag flow is in the negative transport direction: $Q_d = -\frac{1}{2}VHW$ (see Figure 3c). This must be overcompensated by a pressure flow to yield a net transport. Because of continuity of throughput, it follows that

$$Q_p = (1 + f)Q_d \tag{6}$$

In rectangular ducts of width W and height H (the influence of side walls neglected here), the expression for pressure flow for a Newtonian fluid reads [7, 33, 34]

$$Q_p = -\frac{1}{12\mu}\frac{dp}{dz}H^3W \tag{7}$$

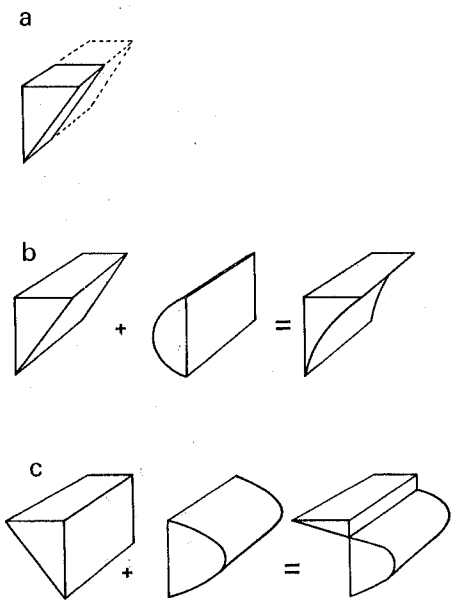

Figure 3. Transport in parts a, b and c.

By substituting in Equations 2 and 7, Equation 4 can now be written as

$$Q = \tfrac{1}{2}VHW - \frac{1}{12\mu}\frac{dp}{dz}H^3W \tag{8}$$

ANALYSIS OF SIMPLIFIED GEOMETRY

Provided that the leads of the forward and reverse zone are numerically equal, that the numbe of flights in all zones is equal, and that the pressure generated in zone "b" is dissipated in zone "c the simplified geometry can now be analyzed.

Relative Lengths

For "a":

$$Q = f\tfrac{1}{2}VHW \tag{9}$$

$$dp/dz = 0 \tag{10}$$

For "b":

$$Q = f\tfrac{1}{2}VHW$$

$$= \tfrac{1}{2}VHW - \frac{1}{12\mu}\frac{dp}{dz}H^3W \tag{11}$$

hence

$$\frac{dp}{dz} = (1-f)\frac{6\mu V}{H^2} \tag{12}$$

For "c":

$$Q = f\tfrac{1}{2}VHW$$

$$= -\tfrac{1}{2}VHW - \frac{1}{12\mu}\frac{dp}{dz}H^3W \tag{13}$$

hence

$$\frac{dp}{dz} = -(1+f)\frac{6\mu V}{H^2} \tag{14}$$

From Equations 12 and 14 it follows that

$$\left.\frac{dp}{dz}\right|_b \Big/ \left.\frac{dp}{dz}\right|_c = -\frac{1-f}{1+f} \tag{15}$$

(The minus sign is because of different signs of pressure gradients in parts "b" and "c".) In case of an isothermal Newtonian fluid, the pressure gradient is constant:

$$\frac{dp}{dz} = \frac{\Delta p}{L} \tag{16}$$

It is now possible to determine the length ratio with Equations 15 and 16:

$$\frac{L_b}{L_c} = \frac{1+f}{1-f} \tag{17}$$

(minus sign omitted.) Let the total length of the screw be L; then

$$L_a = L - L_b - L_c \tag{18}$$

With Equations 17 and 18:

$$L_a = L - \frac{2}{1-f}L_c \tag{19}$$

If relative lengths are defined as

$$\ell_a = \frac{L_a}{L}$$

$$\ell_b = \frac{L_b}{L} \tag{20}$$

$$\ell_c = \frac{L_c}{L}$$

and ℓ_c is given, this yields

$$\left.\begin{aligned} \ell_a &= 1 - \frac{2}{1-f}\ell_c \\ \ell_b &= \frac{1+f}{1-f}\ell_c \\ \ell_c &= \ell_c \end{aligned}\right\} \tag{21}$$

Example: if $f = 0.3$ and $\ell_c = 0.2$, then $\ell_a = 0.43$ and $\ell_b = 0.37$.

Specific Energy

The absolute value of the shear stress (N/m^2) at the wall equals

$$\tau_w = \mu\left|\frac{du}{dy}\right|_{y=H} \tag{22}$$

The absolute value of the shear rate at the wall reads [7, 33, 34]

$$\left|\frac{du}{dy}\right|_{y=H} = \frac{|V|}{H} + \frac{1}{2\mu}\frac{|dp|}{dz}H \tag{23}$$

So, for the three parts "a", "b", and "c" this yields "a"—Equations 10 plus 22 plus 23:

$$\tau_w = \mu\frac{V}{H} \tag{24}$$

"b"—Equations 12, 22 plus 23:

$$\tau_w = \mu\frac{V}{H}(4-3f) \tag{25}$$

"c"—Equations 14, 22 plus 23:

$$\tau_w = \mu\frac{V}{H}(4+3f) \tag{26}$$

The force (N) acting on the wall equals the product of shear stress and surface area where the stress is active.

$$F = f\tau_w\pi DL \tag{27}$$

"a"—Equations 21, 24 plus 27:

$$F = f\cdot\mu\frac{V}{H}\pi DL\left(1 - \frac{2}{1-f}\ell_c\right) \tag{28}$$

"b"—Equations 21, 25 plus 27:

$$F = \mu\frac{V}{H}\pi DL(4-3f)\frac{1+f}{1-f}\ell_c \tag{29}$$

"c"—Equations 21, 26 plus 27:

$$F = \mu \frac{V}{H} \pi DL(4 + 3f)\ell_c \tag{30}$$

The total force is the sum of these three forces:

$$F_t = \mu \frac{V}{H} \pi DLf\left(1 + \frac{2(3f + 4)}{f} \ell_c\right) \tag{31}$$

The torque (Nm) equals the force times the radius:

$$T = F_t \tfrac{1}{2} D \tag{32}$$

The power (Nm/s) is torque times screw speed (rad/s).

$$P = TN2\pi \tag{33}$$

From Equations 31, 32, and 33, it follows that

$$P = \mu \frac{V}{H} \pi^2 D^2 LNF\left(1 + \frac{2(3f + 4)}{f} \ell_c\right) \tag{34}$$

Or (with $|\cos \varphi| \sim 1$ still)

$$f = \frac{Q}{\tfrac{1}{2} VHW}$$

$$V = \pi DN \tag{35}$$

$$W = \pi D \sin \varphi$$

$$P = \frac{2\pi \mu DLNQ}{H^2 \sin \varphi}\left(1 + \frac{2(3f + 4)}{f} \ell_c\right) \tag{36}$$

Without elements "c" with negative pitch, $\ell_c = 0$ so the term between the brackets equals 1 and the normal expression for a single screw extruder is found [35]. With the elements "c", the term between the brackets yields the relative importance of the presence of elements with negative pitch, see Table 1.

The lower the value of f, the more important is the completely filled part (although absolutely smaller because of decreasing L_b because of increasing pressure gradient in part "b") relative to the partly filled channel.

Table 1
Relative Importance of Elements with Negative Pitch: Power Consumption in a Completely Filled Channel (%)

ℓ_c	0.01	0.05	0.1	0.2	0.4
$f = 0.4\ 26\ell_c/(1 + 26\ell_c)$	21	56	72	84	91
$f = 0.3\ 33\ell_c(1 + 33\ell_c)$	25	62	77	87	93
$f = 0.2\ 46\ell_c(1 + 46\ell_c)$	32	70	82	90	95

Another way to illustrate the relative importance of the channel part that is completely filled ($\ell_b + \ell_c$) by the presence of "c" elements is given by the ratio

$$\frac{P_{b+c}}{P_a} = \frac{(4 - 3f)\dfrac{1 + f}{1 - f} + 4 + 3f}{f\left(\dfrac{2}{1 - f}\right)}$$

$$= \frac{4 - 3f^2}{f} \tag{37}$$

Thus: f = (0.4; 0.3; 0.2) yields P_{b+c}/P_a = (9, 13, 20).

For f = 0.3, a part with negative pitch involves the consumption of 13 times the power relative to a partly filled channel "a" of the same length. These simple calculations illustrate the relative importance of negative pitch parts, yet it must be kept in mind that until now, the power consumption in the clearance between flight and cylinder has not been taken into account.

The specific energy (kWh/kg) is power (kW) divided by throughput (kg/h). From Equation 36 and as Q = (m^3/s):

$$Q_m = Q3{,}600\rho \tag{38}$$

This yields

$$E_{sp.} = \frac{\pi \mu DLN}{1.8\ \rho H^2 \sin \varphi}\left(1 + \frac{2(3f + 4)}{f} \ell_c\right) \tag{39}$$

Again Equation 39 yields, for $\ell_c = 0$, the identical result as derived for single-screw extruders.

Scaling

The procedure adopted so far reveals that it is well worth examining what happens during the scaling up from a small extruder to a larger one.

Geometrical Scaling

Usually, corotating twin-screw extruders scale (up to D ~ 200 mm) geometrically; this implies that

$$\frac{H}{D} = \text{constant}$$

$$\frac{L}{D} = \text{constant} \tag{40}$$

$$N = \text{constant}$$

Furthermore (locally),

$$\varphi = \text{constant}$$

$$\ell_c = \text{constant} \tag{41}$$

$$f = \text{constant}$$

These practical rules are based on the principles that keep the mixing constant. Shear rate:

$$\dot{\gamma} \sim \frac{V}{H} \sim \frac{\pi DN}{H} \tag{42}$$

Mean residence time:

$$\bar{t} \sim \frac{\text{volume}}{\text{throughput}} \sim \frac{f_\ell \pi DLH}{Q} \tag{43}$$

$$= \frac{f_\ell \pi DLH}{f\frac{1}{2}VHW} = \frac{f_\ell 2L}{f\pi DN \sin\varphi} \tag{44}$$

with f_ℓ = local degree of fill* (f is the degree of fill, e.g., underneath the hopper used only (instead of Q) as a kind of dimensionless measure for the metered throughput (Equation 3). f_ℓ is the local degree of fill. It is equal to one in the case of completely filled parts, but may differ from f, for example, by a change of pitch.) Total shear:

$$\gamma = \dot{\gamma}\bar{t}$$

$$= \frac{f_\ell 2L}{fH \sin\varphi} \tag{45}$$

As is well known [36], reorientation relative to the direction of shear is extremely important for the mixing efficiency:

$$\text{M.E.} \sim \left(\frac{1}{nr}\gamma\right)^{nr} \tag{46}$$

(The working principle of static mixers is completely based on nr rather than on the total shear γ.) During each revolution of the screw, material is passed from one screw to the other and is (assumed to be) completely reoriented. This may be written as:

$$nr = n \cdot N \cdot \bar{t} \tag{47}$$

where nr = the number of reorientations
n = the number of flights
N = screw revolutions per second
$\bar{t}$ = the mean residence time according to Equation 43

Hence,

$$nr = \frac{2f_\ell \pi DNLH}{Q}$$

$$= 2n\frac{f_\ell L}{f\pi D \sin\varphi} \tag{48}$$

From Equations 40 and 41, it can be seen that the degree of mixing (Equations 42, 44 and 45) remains constant: f, L/D and ℓ_c = constant implies ℓ_b = constant and ℓ_a = constant (Equation 21). If the same material is used (μ, ρ = constant) the specific energy, Equation 39, is also constant. Furthermore, it follows that throughput, energy and torque all scale with the third power of the diameter in this case. See Table 2.

Table 2
Scaling Laws

Definitions			
Screw speed	$\frac{N}{N_0} = \left(\frac{D}{D_0}\right)^n$	Specific energy	$\frac{Esp}{Esp_0} = \left(\frac{D}{D_0}\right)^{es}$
Channel depth	$\frac{H}{H_0} = \left(\frac{D}{D_0}\right)^h$	Throughput	$\frac{Q}{Q_0} = \left(\frac{D}{D_0}\right)^q$
Screw length	$\frac{L}{L_0} = \left(\frac{D}{D_0}\right)^\ell$	Mean residence time	$\frac{\bar{t}}{\bar{t}_0} = \left(\frac{D}{D_0}\right)^t$
Power	$\frac{P}{P_0} = \left(\frac{D}{D_0}\right)^p$	Shear rate	$\frac{\dot{\gamma}}{\dot{\gamma}_0} = \left(\frac{D}{D_0}\right)^g$
Torque	$\frac{M}{M_0} = \left(\frac{D}{D_0}\right)^m$	Total shear	$\frac{\gamma}{\gamma_0} = \left(\frac{D}{D_0}\right)^{gs}$

The usual scaling laws can be derived, either from literature [45, 46, 47] or from the following equations of this chapter.

Equations 2, 35, 36:	$p = 3 + 2n + \ell - h$
Equations 2, 35:	$q = 2 + n + h$
	$es = p - q = 1 + n + \ell - 2h$
Equations 2, 31, 32:	$m = 3 + n + \ell - h$
Equations 1, 35, 44:	$t = h + 1 + \ell - q = \ell - 1 - n$
Equation 42:	$g = n - h + 1$
	$gs = g + t = \ell - h$

The scaling laws result in the following numerical values, depending on the method of scaling (see text, Equations 40 through 60).

	Geometrical	Laminar	Ideally Mixed	
n	0	−1	−0.667	−0.5
h	1	0.5	0.667	1
ℓ	1	1	1	1.5
p	3	1.5	2	2.5
es	0	0	0	0
m	3	2.5	2.667	3
q	3	1.5	2	2.5
t	0	1	0.667	1
g	0	−0.5	−0.333	−0.5
gs	0	0.5	0.333	0.5

Thermal Scaling

Geometrical scaling is allowed only if both extruders are operating under fully adiabatic conditions. As soon as heat exchange with the barrel wall is more important in the process, throughput can only scale with the second power of the diameter because the surface (πDL) scales with D^2. Otherwise, the temperature development in small test extruders will be different from that in larger ones, with all consequences for viscosity differences (mixing!) and thermal degradation with the more recently developed high-melting-point polymers.

The problem that arises is that scaling according to the mixing rules does not provide the same laws as scaling according to the rules of equal thermal development. In practice, this means that choices have to be made and that experiments and eventually changes in screw design on the larger scale extruder will always be necessary. This is illustrated by Figure 4.

In the simplest case, the temperature development is given by

$$\rho c u \frac{\partial T}{\partial x} = \lambda \frac{\partial^2 T}{\partial y^2} + \mu \left(\frac{du}{dy}\right)^2 \tag{49}$$

for laminar flows and by

$$\rho c \bar{u} \frac{d\bar{T}}{dx} = \frac{\langle \alpha \rangle (\bar{T} - T_w)}{H} + \mu \left(\frac{d\bar{u}}{dy}\right)^2 \tag{50}$$

for ideally mixed (pipe) flows, see Figure 4.

The dimensionless form of these equations yields the requirements for equal temperature development. For laminar flows:

$$Gz\, u^* \frac{\partial T^*}{\partial x^*} = \frac{\partial^2 T^*}{\partial y^{*2}} + Br \left(\frac{du^*}{dy^*}\right)^2 \tag{51}$$

$$Gz = \text{Graetz number} = \frac{\rho c V H}{\lambda} \frac{H}{L} \tag{52}$$

and

$$Br = \text{Brinkman number} = \frac{\mu V^2}{\lambda \Delta T} \tag{53}$$

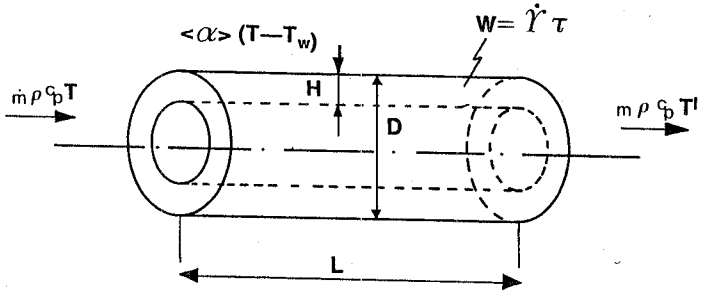

Figure 4. Heat balance for an ideally mixed system.

If Gz- and Br-numbers are constant, solution of Equation 50 always gives the same result. Provided that the same material is used (λ, ρ, c, and μ are constant), the same wall temperature (T_w) is employed, and (as usual) L/D = a constant, then these conditions yield (Equation 53)

$$V = \text{constant; consequently } N \sim D^{-1} \tag{54}$$

And from Equations 52 and 54 it follows that

$$H \sim D^{0.5} \tag{55}$$

These very severe demands result in $Q \sim D^{1.5}$.

The conditions $\ell = 1$, $n = -1$, $h = 0.5$ and $q = 1.5$ (Table 2) are met in practice only when heat exchange with the walls is extremely important, for instance in the melting section of a single-screw extruder with a grooved feed zone [37].

For ideally mixed (annular) flows (Appendix 1), which may be assumed for the radially well mixed flow in corotating twin-screw extruders:

$$P\bar{u}^* \frac{\partial \bar{T}^*}{\partial x^*} = \bar{T}^* + B \left(\frac{d\bar{u}^*}{dy^*}\right)^2 \tag{56}$$

$$\text{P-number} = \frac{\rho c}{\langle \alpha \rangle} \frac{VH}{L} = \frac{\text{Péclet}}{\text{Nusselt}} \tag{57}$$

$$\text{B-number} = \frac{\mu}{\langle \alpha \rangle} \frac{V^2}{H \Delta T} = \frac{\text{Brinkman}}{\text{Nusselt}} * \text{As} \tag{58}$$

where $\text{Nusselt} = \dfrac{\langle \alpha \rangle L}{\lambda}$

$$\text{Péclet} = \frac{\rho c V H}{\lambda}$$

$$\text{As} = \frac{L}{H}$$

Constant temperature developments in this case require constant P- and B-numbers; therefore, using the same material (ρ, c, μ, λ constant), the same heat transfer coefficient $\langle \alpha \rangle$, wall temperature (T_w) and when L/D is constant, $V \sim H^{0.5}$ and VH/D = constant. Hence,

$$V \sim D^{1/3}$$

$$\text{and therefore} \quad N \sim D^{-2/3} \tag{59}$$

$$\text{and} \quad H \sim D^{2/3}$$

For the throughput, this implies, as expected, $Q \sim D^2$.

Consequently: $\ell = 1$, $n = -2/3$, $h = 2/3$, and $q = 2$ (Table 2). The scaling law for channel depth (Equation 59) is often found in practice for many extruders [37], of course, because channel depths

can be determined only once. Screw speeds and throughputs can be changed easily at any moment. If the restriction of L/D = c is dropped, and H ~ D is introduced (as is practice in corotating twin-screw extruders), then the requirement of constant P- and B-numbers yields $V \sim D^{0.5}$ and VD/L = a constant, so $N \sim D^{-0.5}$, $L \sim D^{1.5}$ and H ~ D. Therefore,

$$Q \sim D^{2.5} \tag{60}$$

and $\ell = 1.5$, h = 1, n = −0.5, q = 2.5 (Table 2).

The conclusions drawn from this look at the scaling laws are that geometrical scaling yields maximum throughput and meets the requirements of constant mixing, but results in a different temperature development as soon as the extruders do not operate in a completely adiabatic mode. Consequently, mixing is not the same anymore because viscosities are temperature dependent.

In the case of equal temperature development, screw speed (absolutely) and throughput (relatively) are lower, with as a consequence decreased mixing, energy consumption, and torque. Large extruders (D > 200 mm) do not allow geometrical scaling because the circumferential speed and wear it causes become too high.

IMPROVEMENTS OF THE ANALYSIS

Until now the analysis was relatively naive and only qualitative. Nevertheless, some understanding of the basic working principles has been raised. Some improvements will now be incorporated in the model.

Leakage Flows

In corotating twin-screw extruders, leakage flows are important because they are relatively large in comparison with single-screw extruders with respect to the throughput that is only a part (f) of the maximum theoretical throughput by drag flow. Moreover, the screw speed is absolutely higher than that of single-screw extruders because of its significant contribution to the mixing process. Additionally, in counterrotating twin-screw extruders, leakage flows are relatively important, especially in the rather large calender gap, as was emphasized in the introduction.

So far we have not considered the influence of the flights because we have tried to simplify the treatment as much as possible. Improvements, however, can and will be easily incorporated.

To compensate for the area occupied by flights (double flighted screws in most cases), the channel width should be reduced and replaced in all equations by

$$W = \pi D \sin\varphi(1 - ne) \tag{61}$$

where e is the relative width of the flights and is given by

$$e = W_f/\pi D \sin\varphi \tag{62}$$

where W_f is the flight width measured perpendicular to the flight and n is the number of flights. A typical value of e is 0.1. (For the analysis here in double- or triple-flighted screws, all flights can be added; mixing, which indeed is dependent on the absolute number of flights, is not being analyzed here.)

This corrected value of the channel width must be introduced into all the equations derived so far; among others, this correction directly influences the value of f, the degree of fill, in Equations 2 and 3.

Because of backflow through clearances (simple drag flow is enough to estimate its value because, in general, pressure flows are negligible in narrow channels), the local throughput that must be transported to the die is larger than the metered throughput Q_m. Therefore, Q_m should be replaced by

$$Q = Q_m + Q_L \tag{63}$$

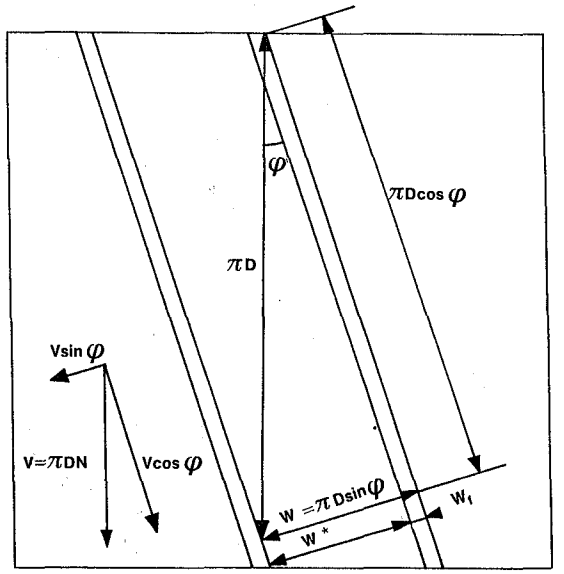

Figure 5. Unrolled screw channel.

with

$$Q_L = \tfrac{1}{2}V\delta\pi D \sin\varphi \cos\varphi(1 - ne) \tag{64}$$

See Figure 5. f is influenced once more by this correction. Having corrected for f, the cos φ that was neglected so far can also be brought in, starting with Equation 1.

Energy Consumption Above the Flights

Above the flights energy is consumed. The shear stress equals

$$\tau = \mu_f \frac{V}{\delta} \tag{65}$$

with μ_f the viscosity above the flight and δ the flight clearance. The surface area A equals

$$A_f = ne\pi DL \tag{66}$$

Therefore, force, torque, and power are, respectively,

$$F_f = \mu_f \frac{V}{\delta} ne\pi DL \tag{67}$$

$$T_f = \tfrac{1}{2}\mu_f \frac{V}{\delta} ne\pi D^2 L \tag{68}$$

$$P_f = \mu_f \frac{V}{\delta} ne\pi^2 D^2 LN \tag{69}$$

A comparison of the power consumed above the flights relative to that in the channels can now be made if Equation 34 is corrected according to Equations 61, 63, and 64 and by the incorporation of cos φ:

$$P_c = \mu_c \frac{V}{H} \pi^2 D^2 L N f \left(1 + \frac{2(3f+4)}{f} \ell_c\right)(1 - ne) \tag{70}$$

and

$$f = \frac{Q}{\frac{1}{2} V \cos\varphi \, HW^*}$$

$$= \frac{Q_m + \frac{1}{2} V \delta \pi D \sin\varphi \cos\varphi (1 - ne)}{\frac{1}{2} V H \pi D \sin\varphi \cos\varphi (1 - ne)} \tag{71}$$

Therefore,

$$f = \frac{Q_m}{\frac{1}{2}\pi^2 D^2 H N \cos\varphi \sin\varphi (1 - ne)} + \frac{\delta}{H} \tag{72}$$

yielding

$$\frac{P_f}{P_c} = \frac{\mu_f}{\mu_c} \frac{H}{\delta} \frac{ne}{(1 - ne)} \frac{1}{(1 + 2(3f+4)\ell_c)} \tag{73}$$

In Equations 65 through 70 and Equation 73, μ_f and μ_c are introduced to allow us to choose a somewhat lower Newtonian viscosity above the flights, caused by pronounced shear thinning and temperature rise due to local dissipation here. With typical data $H/\delta = 40$; $n = 2$; $e = 0.1$; and $\mu_f/\mu_c = 0.15$. As is clearly illustrated in Table 3, power consumption between thhe screw flights and the barrel is large compared to the power consumption in the channel. This is typical for these (usually) low values of degree of fill, f.

Mixing Elements

So far we have only dealt with the simplest combination of screw elements with positive and negative pitch. Moreover, only one screw has been analyzed. The geometry of two combined screws is more complex and many other elements exist, as is illustrated in Figure 6.

Calculation of these elements is now rather straightforward. First, we have to evaluate in more detail the effective channel width to be used in the calculations. Both screws have to be visually investigated simultaneously, preferably in the unrolled state [1, 4, 5, 14]. This yields

$$Q = 2Q_m + Q_L \frac{2n - 1}{n} \tag{74}$$

Table 3
Power Consumption Above Flights in Comparison with Channels (P_f/P_c)

	$\ell_c = 0.01$	0.05	0.1	0.2	0.4
f = 0.4	3.0	1.6	1.0	0.6	0.33
f = 0.3	3.8	1.9	1.2	0.66	0.36
f = 0.2	5.2	2.3	1.3	0.74	0.39

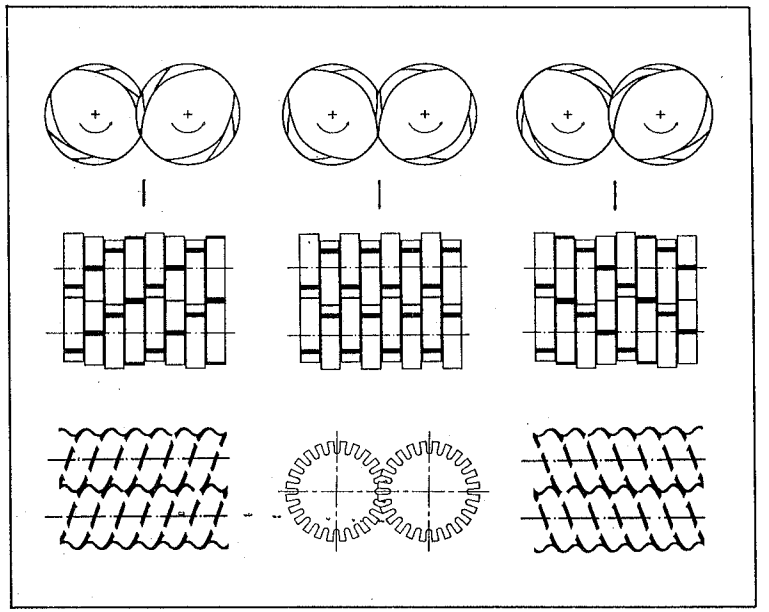

Figure 6. Various mixing and kneading elements.

the total metered throughput corrected for leakage flow over the flights.

$$W = \frac{2n - 1}{n} \pi D \sin\varphi (1 - ne) \tag{75}$$

Second, for the mixing elements, a main pitch angle φ, positive (e.g., 45°), neutral (0°) or "negative" (e.g., 135°) must be recognized. Finally, we must sum up the number of holes in the flight leaving room for positive or negative drag- and pressure flows. If the length of the sum of the remaining screw flight is defined as being a factor r of the total screw flight length ($L_f = r\pi D/\cos\varphi$), the sum of the holes equals the factor $(1 - r)$.

Because of the holes, a leakage by drag flow back into the previous channel exists. Therefore, the throughput should be increased to compensate for this leakage flow:

$$Q = 2Q_m + Q_L \frac{2n - 1}{n} + Q_{LD} \tag{76}$$

with

$$Q_{LD} = \tfrac{1}{2} V H \pi D \sin\varphi \cos\varphi (1 - r) F_N F_D \tag{77}$$

where $F_N = (2n - 1)/(n)(1 - ne)$. F_D is a correction factor, like F_P, that could be used to compensate for the influence of the side walls (the flights) on the drag flow in this case [6, 34, 38], if the ratio of channel depth to channel width is not negligible anymore.

Not only is the throughput influenced because of the holes' presence, but also the pressure gradient in axial direction dominates the one in down-channel direction. We must consider the parallel combination of two resistances, represented by their characteristic cross-sections: The rectangular

screw channel and the passage through the holes. This is reflected in Equations 78 and 79:

$$Q = Q_d + Q_p$$
$$= Q_d - \frac{k}{\mu}\Delta p \tag{78}$$

The factor k can be calculated by

$$k = \left[\frac{1}{12\ell} H^3 \pi D \sin^2 \varphi \, F_N F_P F_{PC} + \frac{1}{12\ell} H^3 \pi D (1 - r) F'_P F_{PC}\right] \tag{79}$$

In a neutral kneading element, for instance, neither flight nor pitch angle can be distinguished (r = 0), so the leakage flow (Equation 76) completely compensates the drag flow (Equation 2) with all the corrections as indicated. In this case, axial pressure gradients are the only transport mechanism. Compare Equation 7.

The flow in the intermeshing region, though not discussed so far, results in an extra contribution to the conveying capacity and can be treated using the description given by Booy [5]. The average contribution, Q_a, per N revolutions to the drag flow is given by

$$Q_a = \frac{\pi}{4} D^3 N \tan \varphi \, k_a \tag{80}$$

with k_a a tabulated function [5].

Table 4
Expressions for Drag and Pressure Flow in Screw Elements
(Based on the total metered throughput, Q.)

Definition:	$Q_{channel} = Q_d + Q_a + Q_p$
	$Q_{channel} = Q_m + Q_L + Q_{LD}$
	$-Q_p = (Q_d + Q_a - Q_L - Q_{LD}) - Q_m$
with	
Pressure flow:	$Q_p = -\frac{k}{\mu}\Delta p$
Drag flow:	$Q_d = \frac{1}{2} V \cos \varphi \, H \pi D \sin \varphi \, F_N F_D F_{DC}$
Flow in the intermeshing region:	$Q_a = \frac{\pi}{4} D^3 N \tan \varphi \, k_a$
Leakage flow (over flights):	$Q_L = \frac{1}{2} V \cos \varphi \, \delta r \, \pi D \sin \varphi \, F_N F_D F_{DC}$
Leakage flow (through flights):	$Q_{LD} = \frac{1}{2} V \cos \varphi \, H(1 - r) \pi D \sin \varphi \, F_N F_D F_{DC}$
$V = \pi DN$; $r = \frac{L_f}{\pi D/\cos \varphi}$; $F_N = \frac{2n-1}{n}(1 - ne)$;	
k_a, F_D, F_P, F_{DC}, F_{PC} [5, 14, 17]	
$k = \left[\frac{1}{12\ell} H^3 \pi D \sin^2 \varphi \, F_N F_P F_{PC} + \frac{1}{12\ell} H^3 \pi D (1 - r) F'_P F_{PC}\right]$	

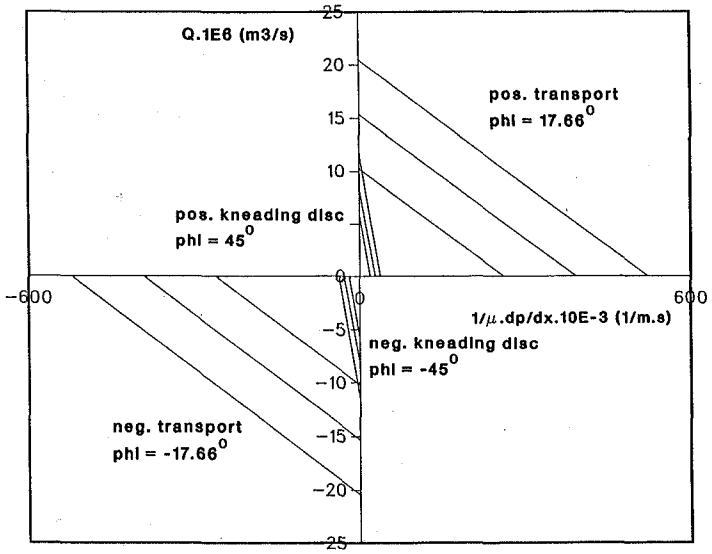

Figure 7. Pressure versus throughput characteristic for transport elements and kneading discs having positive and negative pitch (corotating twin-screw extruder, D = 25 mm). Parameter: screw speed.

In the equations used so far, this term can be brought in:

$$Q = Q_d + Q_a + Q_p$$

The analysis is summarized in Table 4, which yields the expressions for the pressure gradients and volume flows with all corrections brought in so far. Figure 7 shows the throughput versus pressure characteristic for the various screw elements previously mentioned.

All kinds of screw geometries can be modeled now, including screws where no negative pitch elements are present and those screws that consist of any combination of transport, mixing or kneading elements. Before dealing with that, we have to analyze in more detail what happens if several different screw elements are combined sequentially.

Sequence of Screw Elements

In the Newtonian isothermal case with constant viscosity, a combination of different screw elements can be investigated independently of the preceding and following elements. To be more precise: all elements of the same kind can eventually be packed together in order to calculate power and specific energy.

A complete screw like the one in Figure 8 can be dealt with as a pure a, b, d, c screw with a sequence of partly filled parts "a" (with total length equal to the sum of the individual parts "a"), completely filled pressure-generating parts "b", completely filled pressure-generating or pressure-consuming parts "d" (mixing elements), and completely filled pressure-consuming parts "c" (all with total length equal to the sum of their individual components).

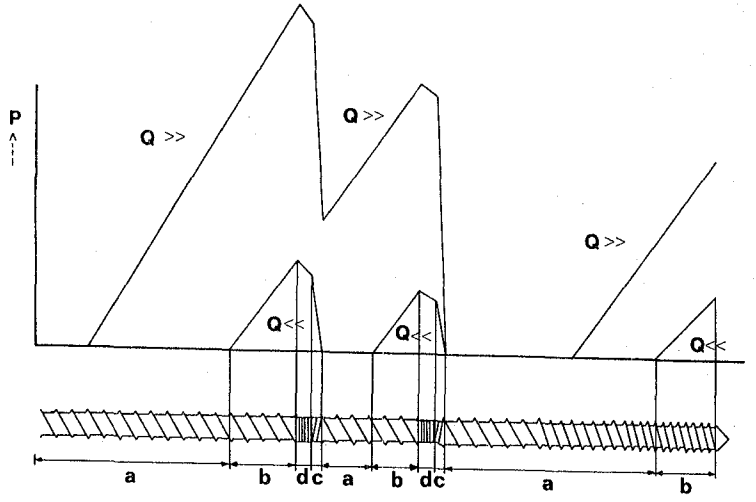

Figure 8. Pressure profiles and filled lengths; parameter: throughput.

If, however, more detailed information is required than only (specific) energy—for instance, if we want to know where the screw is partly filled or where the viscosity changes during extrusion (the non-isothermal, non-Newtonian case)—then only a repetition of the same calculations for the individual sequential components and combinations can give the answers. In all cases, the influence of one element (pressure-consuming) can be noticeable in the preceding sections (in a complex way, because many leakage flows are introduced).

For instance, if a combination (a, b, d, c, a, b, d, c) is used (Figure 8), then with increasing throughput, Q, the length of the second partly filled part "a" might become negative. This means that the pressure buildup capacity of the second part "b" is not enough to compensate for the pressure consumption in parts "d" and "c". As a consequence, the absolute pressure at the end of the first part "c" has a positive value, the first part "b" increases in length to generate this extra pressure and the first part "a" decreases in length.

If even the length of the first part "a" is negative, the screw is no longer able to transport this throughput with this screw design: The critical screw speed has been reached.

Non-Isothermal Power Law Calculations

The isothermal Newtonian treatment of the flow in corotating twin-screw extruders previously mentioned is very successful in providing qualitative information about working principles and consequences of different screw design in the melt section. The best understanding originates from the most simple model. However, quantitative answers cannot be given because the influence of temperature and shear rate on the viscosity (and as a consequence, on local pressure-generating capacity) must be included.

It is beyond the scope of this chapter to give a detailed analysis of the non-isothermal power law modeling, but some general remarks can be made. In principle, the treatment is completely analogous to the Newtonian modeling, but incremental steps over the length of the extruder must be incorporated in order to define a local viscosity depending on local shear rates, local temperature and, in the case of solvent containing melts, local concentrations.

The viscosity of a power law fluid depends on the temperature and on the second invariant of the rate of strain tensor. The components thereof are calculated from the individual drag and pressure flows. The influences of the main drag component $V/H = \pi DN/H$ in the channel and $V/\delta = \pi DN/\delta$ in the clearance between flight and barrel are dominant, at first sight.

With the local viscosity, the local velocity, the velocity gradient, and the pressure gradient are computed. Given the local throughput (Q) and the conservation laws of momentum and mass, it follows that

$$\frac{dp}{dz} = \frac{d}{dy}\left(\mu_0 e^{-b(T-T_0)}\left(\frac{du}{dy}\right)^n\right) \tag{81}$$

$$Q = W\int_0^H u\,dy \tag{82}$$

These equations finally result in a set of two implicit equations for the two unknowns (the pressure gradient and an integration constant). Successful solution of this system (e.g., with a Newton-Raphson procedure) strongly depends upon the first estimate of the values of the two unknowns. A much more convenient way to solve the problem is to write Equation 81 in a different way:

$$\frac{dp}{dz} = \frac{d}{dy}\left(\mu_0 e^{-b(T-T_0)}\left(\frac{du}{dy}\right)^{n-1}\frac{du}{dy}\right) \tag{83}$$

which means

$$\frac{dp}{dz} = \frac{d}{dy}\left(\mu(z, y)\frac{du}{dy}\right) \tag{84}$$

The tri-diagonal matrix resulting from this expression combined with a last row completely filled with the digits 1, 4 and 2, resulting from the discretization of mass continuity (Equation 82) according to a Simpson-like integration rule, results in a straightforward solution. Very fast recursion formulas exist for the composition and solution of tri-diagonal matrices [40], while the last row of the matrix can be brushed simultaneously already during the formation of the tri-diagonal matrix. Besides, an extension to the three dimensional flow field can now be easily incorporated:

$$\frac{\partial p}{\partial z} = \frac{\partial}{\partial y}\left(\mu(z, y)\frac{\partial v_z}{\partial y}\right) \tag{85}$$

$$\frac{\partial p}{\partial x} = \frac{\partial}{\partial y}\left(\mu(z, y)\frac{\partial v_x}{\partial y}\right) \tag{86}$$

$$\mu(z, y) = \mu_0 e^{-b(T-T_0)}\left(\left(\frac{\partial v_z}{\partial y}\right)^2 + \left(\frac{\partial v_x}{\partial y}\right)^2\right)^{(n-1)/2} \tag{87}$$

For this (coupled) system the same tri-diagonal matrix must be solved for both x- and z-directions; the only difference being the boundary condition at the barrel:

$$v_z = V\cos\varphi \qquad v_x = V\sin\varphi \tag{88}$$

Coupling of the equations via the viscosity is not only due to the shear rate dependency but also via the temperature (Equation 87).

The next step, therefore, is calculating the local temperature. This can be performed relatively simply because the flow in the channel is considered to be perfectly mixed (one screw taking over the material from the other while completely reorientating it). Therefore, a local heat balance (Figure 9) dictates that the heat stored in the local volume (resulting in a temperature rise) equals the dissipative heat generated by the velocity gradients plus the heat exchanged with the walls (positive or negative).

The last term is calculated with an average heat transfer coefficient $\langle\alpha\rangle$ multiplied by the temperature difference. This engineering $\langle\alpha\rangle$ is not known a priori, and experiments must yield its value.

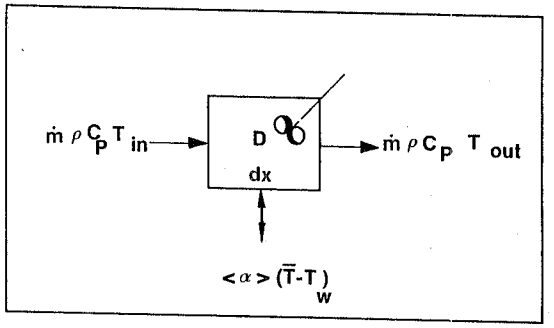

Figure 9. Heat balance for an incremental step.

After the new temperature (T_{out} in Figure 9) has been calculated, the average value of the viscosity is adapted to the average temperature in the volume and calculation of pressure gradients and average temperature is repeated. If the results are not improved anymore (only a few iterations are needed), the next incremental step is taken. See Table 5.

It is recommended not to make the incremental steps too small (a good compromise is one third of the diameter) as the elements are coupled via leakage flows. The calculation must be repeated because of the inflow of material (with another mean temperature) from leakage gaps and following channels.

Moreover, when the calculation is started only analytical estimations of the lengths of parts "a" and "b" are known. Therefore, testing at parts where absolute (atmospheric) pressures are known (degassing houses; feed parts; in the worst case at the end of the die) is necessary to check whether the calculated pressure equals the known pressure. If not, a new guess of the length of element "a" and "b" must be made and the calculations repeated.

Provided that we do not want to look at the fourth decimal place, for one simulation of a complete screw only 15 seconds of CPU time on an IBM 370 (with mathematical coprocessor 4381) will suffice.

Results

As a demonstration, only a limited number of results will be presented here. In the first instance, a comparison of simple isothermal Newtonian calculations with those for the non-isothermal power law case will be made.

Table 5
Nonisothermal Power Law Calculations

Numerical Scheme
1. Newtonian analysis
2. Estimation of lengths
3. Step dz
4. Determination of local pressure gradients
5. Determination of local mean temperature, Figure 9
6. Analysis of leakage flow, average temperature and power consumption
7. Corrections on throughput and mean temperature in the channel because of leakage flow(s)
8. Return to 4, until no changes in mean temperature and pressure gradients occur anymore
9. Return to 3, until checkpoint on absolute pressure is reached
10. If not correct: improved estimation of lengths, return to 2
11. If correct, next screw section or end

In Figure 10 the specific energy for a hot melt extruder is plotted as a function of throughput with parameter the screw speed and/or degree of fill. Figure 11 shows the same plot for the non-isothermal power law calculations. The conclusion of this comparison is that the Newtonian model provides qualitatively the right information: minimum specific energy only at maximum degree of fill. Quantitative predictions, however, can only be made with the more complicated calculations shown in Figure 11. Especially when the influence of a screw modification is to be predicted, only the non-isothermal calculations are important (as experienced in practice) because changes in viscosity through local heat dissipation in one part of the screw have a great influence on the heat dissipation in the following parts.

As a second example, a (local) combination of transport and mixing elements has been investigated: a positive, neutral and negative mixing element as is shown in Figure 12. The difference in pressure gradient in the mixing elements is clearly demonstrated by drawing horizontal lines of *zero pressure* from the end of the mixing element towards the left; the filled length can be determined graphically. The difference in pressure gradient between positive and neutral mixing elements is not very large. However, because of the positive transport, screws with positive kneading elements remain almost empty. This is why those kneading blocks are, in practice, always followed by a screw element or kneading block with a negative pitch. Neutral kneading elements only fill themselves, while a negative pitch is of much greater importance because the local negative pressure gradient causes the extruder to be completely filled over a considerable length.

The third example refers again to devolatilization extruders and reveals the end temperature and specific energy in dependence of processing conditions and materials, Table 6.

From these and many other simulations, it can be stated that the more exact predictions about extrusion behavior can only be obtained when a temperature (great influence) and screw speed (smaller influence) dependent heat transfer coefficient $\langle\alpha\rangle$ is used. It is only the heat transfer coefficient on the polymer side that is responsible for this dependency because a thicker isolating polymer layer is formed with lower wall temperatures, screw speeds, and with greater leakage gaps [41, 42].

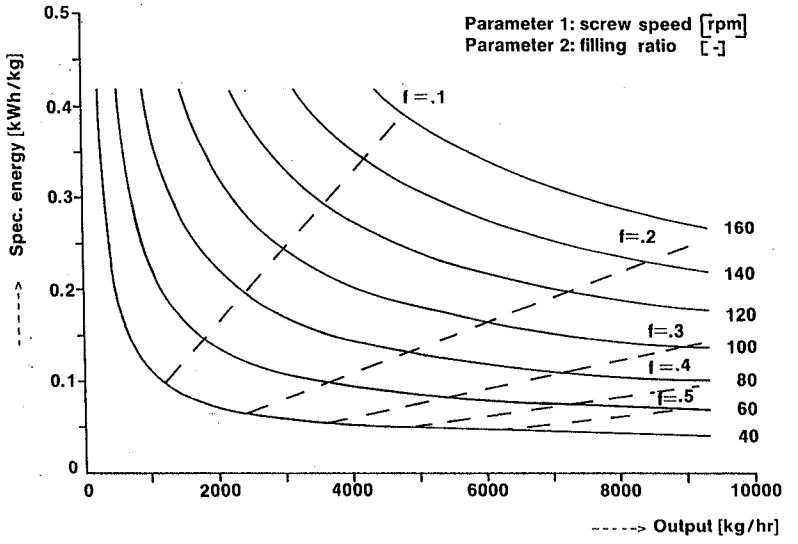

Figure 10. Specific energy as a function of throughput; parameter: screw speed, degree of fill (Isothermal, Newtonian model).

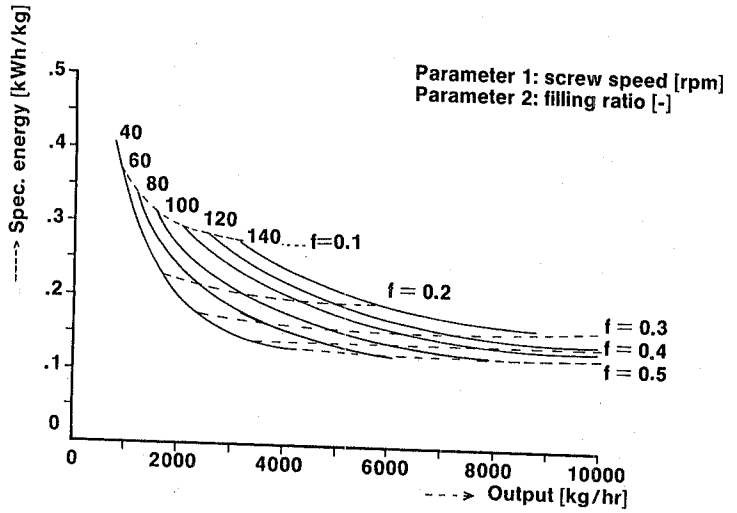

Figure 11. Specific energy as a function of throughput; parameter: screw speed, degree of fill (Nonisothermal, power law model).

Comparison of theoretical predictions and the practical values show a remarkably good correlation. However, we have to realize that an automatic feedback exists. Because of the temperature dependency of the viscosity, a more or less limiting value for the melt temperature and the (specific) energy is present.

The fourth example, therefore, concerns much more direct experiments with model liquids (paraffin oil) in a Plexiglas-walled laboratory extruder. With the setup shown in Figure 13, the combination

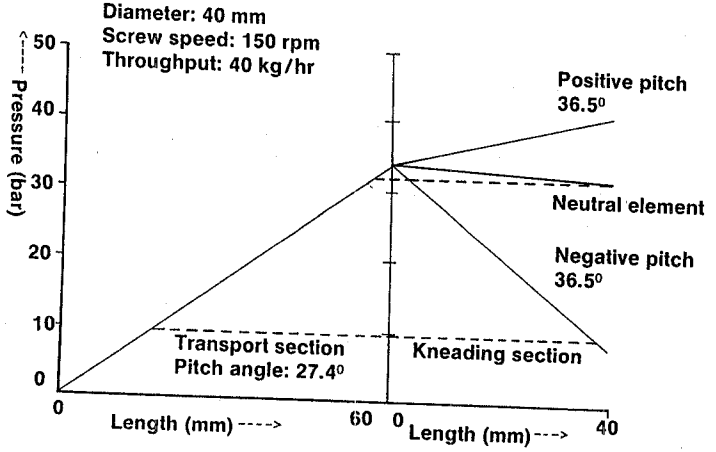

Figure 12. Pressure gradient in a combination of a transport section and kneading sections.

Table 6
Comparison between Final Results from Model Calculations and those from Measurements for a Melt Extruder under Several Processing Conditions.

Viscosity at $\dot{\gamma} = 1$ (Pa·s)	Power law index (−)	Measured values		Calculated values	
		T_{End} (°C)	$E_{spec.}$ (kWh kg^{-1})	T_{End} (°C)	$E_{spec.}$ (kWh kg^{-1})
12,500	0.43	296	0.17	297	0.18
11,300	0.43	292	0.15	294	0.156
10,500	0.43	284	0.137	280	0.148
9,000	0.43	294	0.126	293	0.13
6,250	0.43	286	0.123	287	0.125
485	0.82	228	0.052	224	0.05

of a part c (transport elements having negative pitch or kneading blocks that are neutral or with positive or negative pitch) with transport elements can be investigated directly, compare with the second example. To measure the length of the channel that is completely filled preceding a part c at different screw speeds, a high speed camera was used. Figure 14 shows one image of the film. Figure 15 shows the comparison of calculated and measured filled length for the combination of a transport element having positive pitch with various parts c. Note the large difference in filled length between kneading blocks and transport elements having negative pitch.

The fifth and last example deals with scaling concepts for the glass-fiber reinforcement of a degradation sensitive polymer. Processing should be performed as close as possible to the high melting point (T_m) and, consequently, the scale up rules for equal temperature development should be fulfilled (Table 2). In experiments on two corotating twin-screw extruders with different sizes, the scaling exponents for screw speed and throughput were evaluated. They proved to be dependent, of course, on the requirements that were put on the average temperature of the outcoming melt

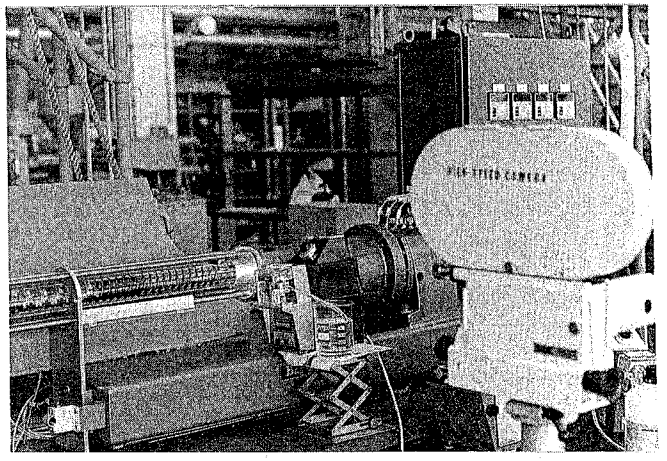

Figure 13. Setup of Plexiglas-walled corotating twin-screw extruder (D = 25 mm) with high speed camera.

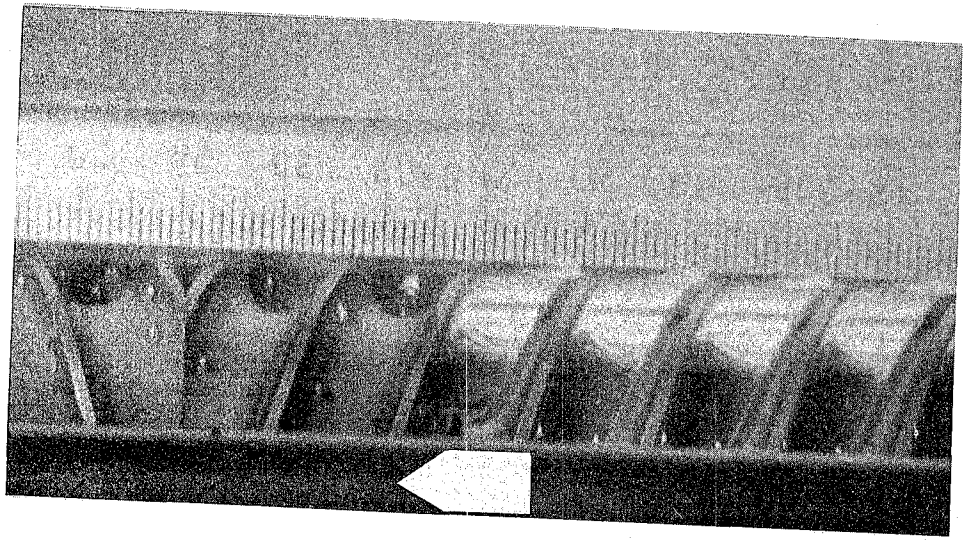

Figure 14. Image of the filled length at a screw speed of 200 rpm.

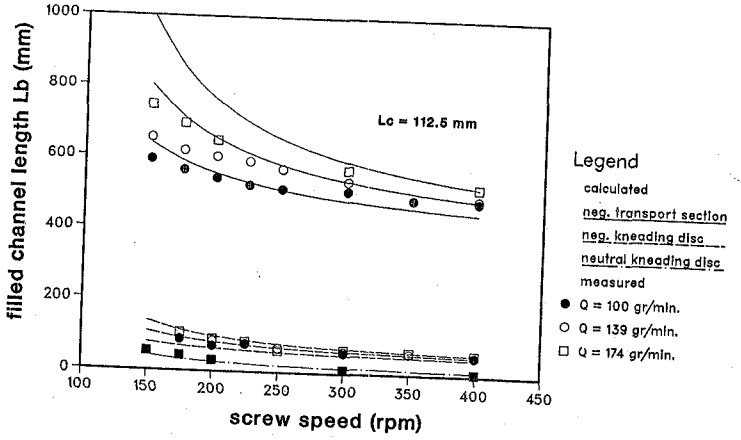

Figure 15. Comparison of calculated and measured filled channel length (L_b) for combinations of transport elements having positive pitch ($\varphi = 17.66°$, $F_D = 0.7$, $F_P = 0.52$, $F_{DC} = 1.02$, $F_{PC} = 1.15$) with transport elements having negative pitch ($\varphi = 180° - 17.66°$, $F_D = 0.7$, $F_{PC} = 0.52$, $F_{DC} = 1.02$, $F_{PC} = 1.15$); kneading discs having negative pitch ($\varphi = 180° - 45°$, $r = 0.23$, $F_D = 0.7$, $F_P = 0.52$, $F_{DC} = 0.88$, $F_{PC} = 0.98$); neutral kneading discs ($\varphi = 0°$, $r = 0$, $F_P = 0.52$, $F_{PC} = 0.75$). L_c (axial) = 112.5 mm in all cases.

(Table 7). Via simulations of the last part of the extruder (melt!), assuming an average melt temperature at the inlet (the end of the melting section), and aiming for the same melt end-temperature on both extruders, $T_m + 25$ in this case, theoretical values for the scaling exponents close to the experimental ones were found (Table 7).

Table 7
Experimental (a, b) and Theoretical (c) Values for the Scaling Exponents for Screw Speed and Throughput

	Average Melt Temperature	Scaling Exponents	
		n	q
a	$T_m + 15$	−1	2.3
b	$T_m + 35$	−0.6	2.5
c	$T_m + 25$	−0.4	2.4

DISCUSSION

It has been shown that a simplified model for a corotating twin-screw extruder is able to predict the correct power consumption, specific energy, and temperature rise, not only over the extruder as a whole, but also locally during the processing (depending on local screw geometry, processing conditions, and material properties). This is of great practical importance in polymer processing because an understanding of the process is within reach and gives a perspective for solving problems in scale up.

The first attempts to visualize the results of the Newtonian calculations have been so far successful. In order to check the non-isothermal, non-Newtonian modeling, experiments to determine critical screw speeds will be performed on a laboratory corotating twin-screw extruder.

Small improvements of the model can be brought in easily, such as:

1. Improvement of the screw geometry used (Equation 10-7 in [13]. See also [1, 4, 14, 43])

$$H(\theta) = \frac{D}{2}(1 + \cos\theta) - \left(L_c^2 - \frac{1}{4}D^2 \sin^2\theta\right)^{1/2} \tag{89}$$

2. A local wall and screw temperature dependent leakage gap (important in large extruders)

An independent determination of the scale-up rules for the heat transfer coefficient is necessary, but most useful will be an incorporation in the modeling of the pressure-generating capacity of the feed section combined with a model of the melting section. Only if these conditions are fulfilled may a complete model exist which, in its turn, could be combined with the existing theory of the dispersion process (for example, [44]) in order to predict the compounding performance for the blending operation.

Acknowledgment

The authors are indebted to G. van Vliet, who originally proposed the basis of this modeling and to H. Lardinoye, G. Kremer and K. Verbraak for the more complex modeling and the computer simulations.

APPENDIX

Heat balance (for length dx):

$$\rho c\bar{u}\frac{d\bar{T}}{dx}dx\pi DH = \langle\alpha\rangle(\bar{T} - T_w)\pi D\,dx + \mu\left(\frac{d\bar{u}}{dy}\right)^2 \pi DH\,dx$$

$$\rho c\bar{u}\frac{d\bar{T}}{dx} = \frac{\langle\alpha\rangle(\bar{T} - T_w)}{H} + \mu\left(\frac{d\bar{u}}{dy}\right)^2$$

In order to make these equations dimensionless, let

$$\bar{u}^* = \frac{\bar{u}}{V}$$

$$\bar{T}^* = \frac{\bar{T} - T_w}{\Delta T}$$

$$dx^* = \frac{dx}{L}$$

$$\rho c \bar{u}^* V \frac{d\bar{T}^*}{dx^*} \cdot \frac{\Delta T}{L} = \frac{\langle\alpha\rangle \bar{T}^* \Delta T}{H} + \frac{\mu V^2}{H^2}\left(\frac{d\bar{u}^*}{dy^*}\right)^2$$

$$\frac{\rho c V H \bar{u}^*}{\langle\alpha\rangle c} \frac{d\bar{T}^*}{dx^*} = \bar{T}^* + \frac{\mu V^2 H}{\langle\alpha\rangle \Delta T H^2}\left(\frac{d\bar{u}^*}{dy^*}\right)^2$$

$$P \cdot \bar{u}^* \frac{d\bar{T}^*}{dx^*} = \bar{T}^* + B\left(\frac{d\bar{u}^*}{dy^*}\right)^2$$

with

$$\text{P number} = \frac{\rho c}{\langle\alpha\rangle} \frac{VH}{L}$$

$$= \frac{\text{Péclet}}{\text{Nusselt}}$$

$$\text{B number} = \frac{\mu}{\langle\alpha\rangle} \frac{V^2}{H\Delta T}$$

$$= \frac{\text{Brinkman}}{\text{Nusselt}} A_s$$

$$\text{Nusselt} = \frac{\langle\alpha\rangle L}{\lambda}$$

$$\text{Péclet} = \frac{\rho c V H}{\lambda}$$

$$A_s = \frac{L}{H}$$

NOTATION

A	surface, m^2
B	coefficient in Equation 56,
Br	Brinkman number,
D	diameter, m
P	power, W
F	force, N
F_x	correction factors (F_d, F_p, F_i, F_N)
Gz	Graetz number,
H	channel depth, m
L	length, m
T	torque, Nm
N	screw speed, s^{-1}
P	coefficient in Equation 56
Q	throughput, $m^3 \cdot s^{-1}$

T	temperature, °C
V	circumferential speed, $m \cdot s^{-1}$
W	channel width, m
b	temperature coefficient of viscosity, K^{-1}
c	specific heat, $J \cdot kg^{-1} \cdot K^{-1}$
e	relative flight width,
f	degree of fill,
k	geometrical factor, m^3
k	tabulated function, Equation 80
ℓ	(relative) length,
n	number of flights,
n	power law index,
nr	number of reorientations,
p	pressure, Pa
r	relative flight length,
t	(average) residence time, s
u, v	velocity, $m \cdot s^{-1}$
x, y, z	coordinates, m
$\langle\alpha\rangle$	average heat transfer coefficient, $W \cdot m^{-2} \cdot K^{-1}$
$\dot{\gamma}$	shear rate, s^{-1}
γ	total shear,
δ	(flight) clearance, m
θ	circumferential angle (Equation 89), rad
λ	heat conduction coefficient, $J \cdot m^{-1} \cdot K^{-1}$
μ	viscosity, Pa·s
ρ	density, $kg \cdot m^{-3}$
τ	shear stress, $N \cdot m^{-2}$
φ	pitch angle,

Subscripts

a	average, Q_a, k_a
a, b, c	part a, b, c, L_a, ℓ_a
c	channel, P_c, μ_c
d	drag, Q_d
D	drag, F_D
DC	drag, curvature, F_{DC}
f	flight, P_f, T_f, F_f, μ_f
i	intermeshing region, F_i
L	leakage, Q_L
ℓ	local, f_ℓ
m	mass, Q_m
m	melt, T_m
N	number of flights, F_N
o	reference, μ_o
P	pressure, F_P
p	pressure, Q_p
PC	pressure, curvature, F_{PC}
sp	specific, E_{sp}
t	total, F_t
x, z	x, z direction, v_x, v_z
w	wall, τ_w

Superscripts

e	energy
es	specific energy,
g	shear rate,
gs	total shear,
h	channel depth,
ℓ	screw length,
m	torque,
n	screw speed,
q	throughput,
t	mean residence time,
( )*	dimensionless, u*
( )* · **	corrected, Q**
$\bar{(\ )}$	average, $\bar{T}$

REFERENCES

1. Szydlowski, W., Brzoskowski, R., and White, J. L., *Int. Pol. Proc.*, *1*, 207 (1987).
2. White, J. L., and Min, K., Paper presented at the European Symposium on Polymer Blends, Strasbourg, France (May 1987).
3. Booy, M. L., *Pol. Eng. Sci.*, *18*, 973 (1978).
4. Werner, H., Ph.D. Thesis, Munich University of Technology, West Germany (1976).
5. Booy, M. L., *Pol. Eng. Sci.*, *20*, 1220 (1980).
6. *Engineering* (London), *114*, 606 (1922).
7. Rowell, H. S., and Finlayson, D., *Engineering* (London), *126*, 249, 385 (1928).
8. Rauwendaal, C. J., *Pol. Eng. Sci.*, *21*, 1092 (1981).
9. Herrmann, H., and Burckhardt, U., *Kunststoffe*, *68*, 753 (1978).
10. Herrmann, H., and Burckhardt, U., *Kunststoffe*, *68*, 19 (1978).
11. Eise, K., Jakopin, S., Hermann, H., Burckhardt, U., and Werner, H., *Adv. Plast Techn.*, 18 (April 1978).
12. Burckhardt, U., Herrmann, H., and Jakopin, S., *Plast. Compounding*, Nov./Dec. 73 (1978).

13. Booy, M. L., *Pol. Eng. Sci., 15*, 606 (1975).
14. Rauwendaal, C. J., *Polymer Extrusion*, Hanser Publishers, Munich (1986).
15. Jansen, L. P. B. M., *Twin-screw Extrusion*, Elsevier, Amsterdam, (1978).
16. Chella, R., Foster, R. W., and Lindt, J. T., Paper presented at the 3rd Meeting of the PPS, Stuttgart, West Germany (April 1987).
17. McKelvey, J. M., *Polymer Processing*, John Wiley & Sons, New York (1962).
18. Tadmor, Z., and Gogos, C. G., *Principles of Polymer Processing*, John Wiley & Sons, New York (1979).
19. Middleman, S., *Fundamentals of Polymer Processing*, McGraw Hill, New York (1977).
20. Noordermeer, J., Proceedings International Conference on Rheology, Acapulco, Mexico (1985).
21. Tokita, N., and White, J. L., *J. Appl. Pol. Sci., 10*, 1011 (1966).
22. White, J. L., and Tokita, N., ibid., *12*, 1589 (1968).
23. Manas-Zloczower, I., Nir, A., and Tadmor, Z., *Rubber Chemistry and Technology, 55*, 1250 (1982).
24. Manas-Zloczower, I., Nir, A., and Tadmor, Z., *Rubber Chem. & Techn., 57*, 583 (1984).
25. Manas-Zloczower, I., Nir, A., and Tadmor, Z., "Dispersive Mixing in Two Roll Mills" (private comm.)
26. Gosler, H., (Werner & Pfleiderer), private communications.
27. Maddock, B. H., SPE ANTEC 383 (1959).
28. Tadmor, Z., *Pol. Eng. Sci., 6* 185 (1966).
29. Ingen Housz, J. F., Meijer, H. E. H., *Pol. Eng. Sci., 21* 352 (1981).
30. Ingen Housz, J. F., Meijer, H. E. H., *Pol. Eng. Sci., 21* 1156, (1981).
31. Tadmor, Z., Hold, P., Valsamis, L., SPE ANTEC 193 (1979).
32. Nordmeier, K., Ph.D. Thesis, Aachen University of Technology, West Germany (1986).
33. Carley, J. F., Mallouk, R. S., and McKelvey, J. M., *Ind. Eng. Chem., 45*, 974 (1953).
34. Carley, J. F., and Strub, R. A., *Ind. Eng. Chem., 45*, 970 (1953).
35. Mallouk, R. S., and McKelvey, J. M., *Ind. Eng. Chem., 45*, 987 (1953).
36. Ng, K. Y., and Erwin, L., *Pol. Eng. Sci., 21*, 4 (1981).
37. Fischer, P., Ph.D. Thesis, Aachen University of Technology, West Germany (1976).
38. Denson, C. D., and Hwang, B. K., *Pol. Eng. Sci., 20*, 965 (1980).
39. White, J. L., and Szydlowski, W., *Adv. Polym. Techn., 7*, 419–426 (1987).
40. Pearson, J. R. A., and Richardson, S. M., (ed.), "Computational Analysis of Polymer Processing," *Appl. Sci.* London (1983).
41. Jepson, *Ind. Eng. Chem., 45*, 992 (1953).
42. Janeschitz-Kriegl, H., and Schijf, J., *Plastics & Polymers*, Dec., 523 (1969).
43. Erdmenger, R., *Chem. Ing. Techn., 36*, 175 (1964).
44. Elmendorp, J. J., Ph.D. Thesis, Delft University of Technology (1986).
45. Ingen Housz, J. F., Intern. Zeitschrift für Lebensmittel Technologie, *1/82*, 48 (1982).
46. Ingen Housz, J. F., Polymer Extrusion II, Paper 8, London (1982).
47. Pearson, J. R. A., *Plast. Rubber Processing*, Sept, 119 (1976).

CHAPTER 13

DEGRADATION OF POLYMERS DURING PROCESSING

G. E. Zaikov and **V. M. Gol'dberg**

Institute of Chemical Physics
Academy of Sciences of the USSR
Moscow, USSR

CONTENTS

INTRODUCTION

The mechanodegradation of polymers in melts has been analyzed in terms of free radical processes. Changes in molecular weight only occur at the chain propagation step. A kinetic scheme accounts for the following characteristics: smooth dependence of molecular weight on temperature in model conditions and a sinusoidal dependence in processing, a decrease in the width of the molecular weight distribution function, a quantitative correlation between ruptures and crosslinks on the one hand, and change in double bond concentration on the other, and an increase in long-chain branching due to the reaction of chain-side radicals. The effects of processing conditions (oxygen, inhibitor, fillers, type of equipment, etc.) are shown.

The mechanism of the chemical reactions that occur during the processing of polymers has been of intense interest because of the practical importance of the problem. Prior to practical application,